Tribology International 43 (2010) 1751–1759

Contents lists available at ScienceDirect

Tribology International

journal homepage: www.elsevier.com/locate/triboint

Stability characteristics of an externally adjustable fluid film bearing in the laminar and turbulent regimes

B.S. Shenoy *, R. Pai

Department of Mechanical and Manufacturing Engineering, Manipal Institute of Technology, Manipal 576 104, Karnataka, India

ARTICLE INFO

Article history:
Received 12 June 2009
Received in revised form
17 April 2010
Accepted 19 April 2010
Available online 24 April 2010

Keywords:
Externally adjustable fluid film bearing
Turbulence
Stiffness and damping
Stability

ABSTRACT

This paper deals with the effect of turbulence on stability characteristics of an externally adjustable fluid film bearing having a design configuration as illustrated by Shenoy and Pai. The time dependent form of Reynolds equation is solved numerically using the finite-difference method. Linearized turbulence model of Ng and Pan is incorporated in the solution scheme. Dynamic coefficients are determined using the method of linearization of bearing reactions. A study with various adjustments predicts that a bearing with negative radial and negative tilt adjustment configuration and operating in turbulent regime results in superior stability as compared to a conventional fluid film bearing.

1. Introduction

Stability of a fluid film bearing depends upon its dynamic coefficients which in turn can be altered by varying the operating parameters like film thickness, eccentricity ratio and journal speed in association with physical properties of the lubricants. However, according to Pai and Parkins [1], a reduction in the bearing clearance will result in significant penalties like reduction in film thickness, increase in heat generation and thermal distortion and therefore places a limit on the value of the radial clearance.

Circular bearings can only offer a little improvement of the static and dynamic performances particularly stiffness and stability. Attention was therefore directed to non-circular forms like lemon bore, offset half, pressure dam and multi-lobe bearings by Akkok and Ettles [2], Schuller [3,4], Malik et al. [5,6]. The notable feature of all these types is their contributions to the improvement of stiffness and stability; they are therefore called the anti-whirl, multi-film bearings by Malik [7], Akkok et al. [8], Soni et al. [9]. All such bearings, however, retain the essential characteristic of being reactive to the operating loads and conditions. Thus, the bearing surface position cannot be altered once manufactured and put in operation. Hence, the adjustable pad bearing is one option to address this issue.

Martin's [10] study was the first for a continuously adjustable pad bearing. He outlined the principles of thermo-hydrodynamic lubrication and viscosity variations, together with an expanded version of the governing pressure field equation as related to the novel adjustable hydrodynamic fluid film bearing. Martin and Parkins [11,12] theoretically and experimentally proved that a continuously adjustable bearing has superior performance characteristics. Martin [13,14] predicted the operating characteristics of one form of continuously adjustable hydrodynamic bearing and designed a multi-body dynamics rig for testing a novel rotor fluid film bearing system. Recently, Shenoy and Pai [15,16] studied the static performance of an externally adjustable fluid film bearing. The design configuration considered by Shenoy and Pai [15,16], as shown in Fig. 1, has a cantilevered externally adjustable bearing element that can be given an independent and controlled position inputs along the radial direction as well as about its leading edge, irrespective of the operating conditions.

This paper deals with a theoretical approach to determine the effect of turbulence on stability characteristics of an externally adjustable fluid film bearing having a design configuration as illustrated by Shenoy and Pai [15,16]. A study with various adjustments predicts that a bearing with negative radial and negative tilt adjustment configuration, which is operating in turbulent regime, results in superior dynamic characteristics as compared to a conventional fluid film bearing.

2. Theory

Pressure distribution in the clearance space between journal and bearing is governed by Reynolds equation. Turbulent flow in a hydrodynamic bearing can be modeled by introducing 'turbulence coefficients' into the Reynolds equation.

$$\frac{\partial}{\partial x}\left[\frac{1}{k_\theta}h^3\frac{\partial p}{\partial x}\right]+\frac{\partial}{\partial z}\left[\frac{1}{k_z}h^3\frac{\partial p}{\partial z}\right]=\frac{1}{2}U\eta\frac{\partial h}{\partial x}+\eta\frac{\partial h}{\partial t} \quad (1)$$

* Corresponding author. Tel.: +91 8202925462; fax: +91 8202571071.
E-mail addresses: satishshenoyb@yahoo.com (B.S. Shenoy), rbpai@yahoo.com (R. Pai).

0301-679X/$ - see front matter © 2010 Elsevier Ltd. All rights reserved.
doi:10.1016/j.triboint.2010.04.015

Nomenclature

C	Radial clearance (m)
C_{xx}, C_{yy}	Direct damping coefficients (Ns/m), $\overline{C}_{xx}=C\omega C_{xx}/W$, $\overline{C}_{yy}=C\omega C_{yy}/W$
C_{xy}, C_{yx}	Cross-coupled damping coefficients (Ns/m), $\overline{C}_{xy}=C\omega C_{xy}/W$, $\overline{C}_{yx}=C\omega C_{yx}/W$
E	Adiabatic parameter $(2\omega\beta\eta_i/c_p\rho g)(R/C)^2$
K_{xx}, K_{yy}	Direct stiffness coefficients (N/m), $\overline{K}_{xx}=CK_{xx}/W$, $\overline{K}_{yy}=CK_{yy}/W$
K_{xy}, K_{yx}	Cross-coupled stiffness coefficients (N/m), $\overline{K}_{xy}=CK_{xy}/W$, $\overline{K}_{yx}=CK_{yx}/W$
L	Length of the bearing (m)
R	Radius of the journal (m)
S	Sommerfeld number, $S=(R/C)^2(\eta N/P)$
Re	Global Reynolds number (ratio of inertia to viscous force), $\mathrm{Re}=R\omega C\rho/\eta_i$
Re_L	Local Reynolds number, $\mathrm{Re}_L=(R\omega C\rho/\eta_L)\overline{h}$
T	Temperature (°C)
T_i	Inlet temperature (°C)
O	Bearing center
O'	Journal center
U	Peripheral velocity of the journal (m/s), $U=\omega R$
W	Load carrying capacity (N), $\overline{W}=WC/\eta_i\omega R^2L$
c_p	Heat capacity (kJ/kg °C)
e	Eccentricity (m), $\varepsilon=e/C$
g	Gravitational constant
h	Film thickness (m), $\overline{h}=h/C$
m_a	Mass of the rotor (kg), $M_a=Cm_a\Omega^2/W$
P	Steady state film pressure (N/m^2), $\overline{p}=pC^2/\eta_i\omega R^2$
t	Time (s)
x	Coordinate axis along circumferential direction (m), $x=R\theta$
Δx, Δy	Displacements of the shaft away from quasi-static position (m)
Z	Coordinate axis along the axial direction (m), $\overline{z}=\frac{z}{L}$
$(M_a)_{cr}$	Dimensionless critical mass parameter $(M_a)_{cr}=(Cm_a\omega^2/W)(\overline{\Omega})_{cr}^2$
$\overline{p}_x$, $\overline{p}_z$,$\overline{p}_{\dot{x}}$, $\overline{p}_{\dot{z}}$	Perturbation pressures
R_{adj}	Normalized radial adjustment, *Radial adjustment*/C
T_{adj}	Normalized tilt adjustment, *Tilt adjustment*/C
$\overline{\Omega}$	Whirl ratio, $\overline{\Omega}=\Omega/\omega$
$(\overline{\Omega})_{cr}$	Dimensionless critical speed
φ_0	Angle of the line of centers with the load line (rad)
η	Lubricant viscosity (Ns/m^2), $\overline{\eta}=\eta/\eta_i$
η_i	Lubricant viscosity at inlet (Ns/m^2)
η_L	Local viscosity of lubricant (Ns/m^2)
θ, θ'	Angular coordinates in the bearing (rad)
θ_1, θ_2	Angles of start and end of hydrodynamic film (rad)
ω	Angular velocity of the journal (rad/s)
ψ	Assumed attitude angle (rad)
δ	Tilt angle (rad)
ρ	Density (kg/m^3)
β	Temperature coefficient of viscosity, $\beta=\ln(\eta_{REF}/\eta_i)(T_i-T_{REF})$
$()_0$	Terms evaluated at quasi-steady-state position
$\dot{()}$,$\ddot{()}$	Dots indicate time derivatives

Lubricant film profile was determined by superimposing the effect of tilt and radial adjustments on the conventional expression for the film thickness [16].

$$\overline{h}=1+\varepsilon\cos(\theta-\psi)+R_{adj}+T_{adj} \tag{2}$$

The bearing operates in the turbulent regime due to higher operating speeds. As in Taylor and Dowson [17], this paper utilizes the Ng and Pan [18] linearized turbulence model. Coefficients k_θ and k_z are calculated using

$$k_\theta=12+k_x(\mathrm{Re}_L)^{n_x} \tag{3}$$

$$k_z=12+k_{zz}(\mathrm{Re}_L)^{n_z} \tag{4}$$

Coefficients k_θ and k_z, in Eqs. (3) and (4), are the functions of local Reynolds number and values of parameters k_x, n_x, k_{zz} and n_z are taken from Taylor and Dowson [17].

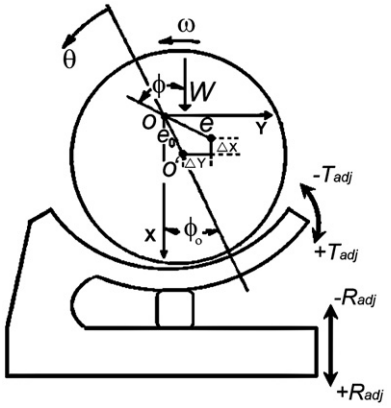

Fig. 1. Schematic diagram of adjustable pad.

A simplified adiabatic model proposed by Pinkus and Bupara [19] is employed to study the effect of temperature on the bearing performance. This adiabatic model [19] assumes an exponential relationship between viscosity and temperature. This model [19] further relates the temperature within the film at any angular position to the film thickness in the circumferential direction thereby using adiabatic parameter '*E*', which is a function of bearing's operating parameters ω, C, R and the lubricant properties c_p, ρ, β and g. Parameters required for the present analysis are taken from Martin [10].

$$\overline{\eta}=e^{-\beta(T-T_i)} \tag{5a}$$

$$T-T_i=\frac{1}{\beta}\ln\left(1+E\int_{\theta_1}^{\theta_2}\frac{d\theta}{(\overline{h})^2}\right) \tag{5b}$$

3. Dynamic equations

Dynamic equations, Eqs. (6)–(10), are derived based on the model [20] of linearization of bearing reactions. Fluid film stiffness and damping coefficients for a perfectly aligned journal are obtained by integrating the dynamic pressures evaluated from Eqs. (7)–(10).

$$\frac{\partial}{\partial\theta}\left(\frac{\overline{h}_0^{\,3}}{k_\theta}\frac{\partial\overline{p}_0}{\partial\theta}\right)+\left(\frac{R}{L}\right)^2\frac{\partial}{\partial\overline{z}}\left(\frac{\overline{h}_0^{\,3}}{k_z}\frac{\partial\overline{p}_0}{\partial\overline{z}}\right)=\frac{\overline{\eta}}{2}\frac{\partial\overline{h}_0}{\partial\theta} \tag{6}$$

$$\frac{\partial}{\partial\theta}\left(\frac{\overline{h}_0^{\,3}}{k_\theta}\frac{\partial\overline{p}_x}{\partial\theta}\right)+\left(\frac{R}{L}\right)^2\frac{\partial}{\partial\overline{z}}\left(\frac{\overline{h}_0^{\,3}}{k_z}\frac{\partial\overline{p}_x}{\partial\overline{z}}\right)$$

$$= \frac{1}{C}\left[-\frac{\overline{\eta}}{2}\left(\sin\theta' + \frac{3\cos\theta'}{\overline{h}_0}\frac{\partial \overline{h}_0}{\partial\theta}\right) + \frac{3\overline{h}_0}{k_\theta}\frac{\partial \overline{p}_0}{\partial\theta}\left(\overline{h}_0\sin\theta' + \cos\theta'\frac{\partial \overline{h}_0}{\partial\theta}\right)\right] \tag{7}$$

$$\frac{\partial}{\partial\theta}\left(\frac{\overline{h}_0^{\,3}}{k_\theta}\frac{\partial \overline{p}_z}{\partial\theta}\right) + \left(\frac{R}{L}\right)^2\frac{\partial}{\partial\overline{z}}\left(\frac{\overline{h}_0^{\,3}}{k_z}\frac{\partial \overline{p}_z}{\partial\overline{z}}\right) = \frac{1}{C}\left[\frac{\overline{\eta}}{2}\left(\cos\theta' - \frac{3\sin\theta'}{\overline{h}_0}\frac{\partial \overline{h}_0}{\partial\theta}\right) - \frac{3\overline{h}_0}{k_\theta}\frac{\partial \overline{p}_0}{\partial\theta}\left(\overline{h}_0\cos\theta' - \sin\theta'\frac{\partial \overline{h}_0}{\partial\theta}\right)\right] \tag{8}$$

$$\frac{\partial}{\partial\theta}\left(\frac{\overline{h}_0^{\,3}}{k_\theta}\frac{\partial \overline{p}_{\dot{x}}}{\partial\theta}\right) + \left(\frac{R}{L}\right)^2\frac{\partial}{\partial\overline{z}}\left(\frac{\overline{h}_0^{\,3}}{k_z}\frac{\partial \overline{p}_{\dot{x}}}{\partial\overline{z}}\right) = \left(\frac{\overline{\eta}}{C\omega}\right)\cos\theta' \tag{9}$$

$$\frac{\partial}{\partial\theta}\left(\frac{\overline{h}_0^{\,3}}{k_\theta}\frac{\partial \overline{p}_{\dot{z}}}{\partial\theta}\right) + \left(\frac{R}{L}\right)^2\frac{\partial}{\partial\overline{z}}\left(\frac{\overline{h}_0^{\,3}}{k_z}\frac{\partial \overline{p}_{\dot{z}}}{\partial\overline{z}}\right) = \left(\frac{\overline{\eta}}{C\omega}\right)\sin\theta' \tag{10}$$

4. Stability margin

The stability margin of the rotor-bearing system is defined in terms of the dimensionless critical mass, $(M_a)_{cr}$, of the journal. At the threshold of instability, $(M_a)_{cr}$ and $(\overline{\Omega})_{cr}$ are calculated, respectively, from

$$(M_a)_{cr} = \frac{(C_{xx}K_{yy} + C_{yy}K_{xx} - C_{yx}K_{xy} - C_{xy}K_{yx})}{C_{xx} + C_{yy}} \tag{11}$$

$$(\overline{\Omega})_{cr}^2 = \frac{[K_{xx} - (M_a)_{cr}][K_{yy} - (M_a)_{cr}] - K_{xy}K_{yx}}{C_{xx}C_{yy} - C_{xy}C_{yx}} \tag{12}$$

If M_a is smaller than $(M_a)_{cr}$, the system will be stable. However, it will be unstable when M_a is larger than $(M_a)_{cr}$. Thus whether the bearing is susceptible to instability obviously depends on the values of the bearing coefficients, which in turn depend on the bearing type and the various performance parameters of these bearings.

5. The boundary condition

Pressure along the bearing edges was set to zero. Cavitation was allowed to occur at ambient pressure by setting all calculated negative pressure equal to zero throughout the iterative solution scheme [16]. This implies that the lubricant film ruptures and reforms when

$$\overline{p} = \frac{\partial \overline{p}}{\partial\theta} = 0 \tag{13}$$

6. The solution procedure

Initially, the lubricant film profile for a given adjustment configuration and an assumed value of attitude angle, (ψ), is determined from Eq. (2). The steady state pressure distribution is evaluated from Eq. (6) satisfying the boundary conditions. Linearized turbulence model of Ng and Pan [18] as well as a simplified adiabatic model of Pinkus and Bupara [19] is implemented in the solution process. A computer code was developed to determine the performance characteristics of the bearing. The finite-difference approximation scheme was adopted and a solution of the resulting set of simultaneous equations was obtained by the Gauss–Seidel method with successive over relaxation. Cavitation is modeled [16] by setting all calculated negative pressure and their gradients equal to zero throughout the iteration. The iteration is repeated until the pressure satisfies the following convergence criterion:

$$\left|\frac{\left\{\overline{p}_{i,j}\right\}_{present\ iteration} - \left\{\overline{p}_{i,j}\right\}_{previous\ iteration}}{\left\{\overline{p}_{i,j}\right\}_{present\ iteration}}\right| \le 0.001$$

On achieving the pressure convergence, static load and the corresponding attitude angle (ϕ_0) are evaluated from the pressure distribution. The resulting attitude angle (ϕ_0) is compared with the assumed value of the attitude angle (ψ). The value of ψ is modified with a small increment of $\Delta\psi$ (i.e., $\psi = \psi + \Delta\psi$) in Eq. (2) and Eq. (6) is solved using this modified value until ψ converges to ϕ_0.

Furthermore, on achieving the convergence of both steady state pressure and attitude angle, perturbation pressures are calculated by substituting the steady state pressure in Eqs. (7)–(10) and solving them, iteratively. Dynamic coefficients are then evaluated from these perturbation pressures. Dimensionless critical mass $(M_a)_{cr}$ and whirl frequency ratio $(\overline{\Omega})_{cr}$ are evaluated from Eqs. (11) and (12), respectively.

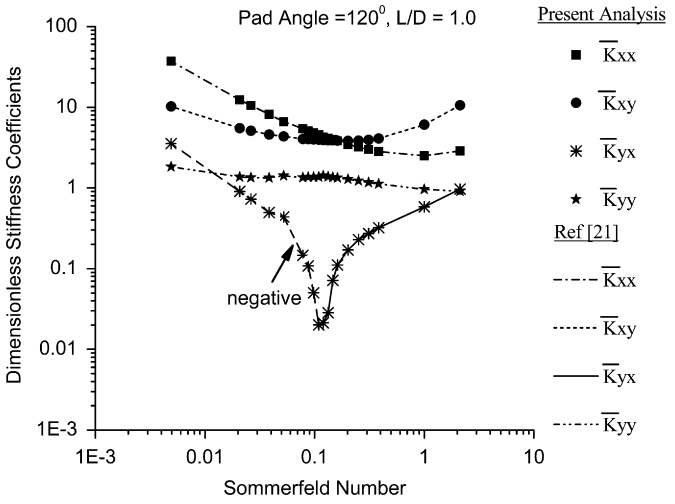

Fig. 2. Comparison of dimensionless stiffness coefficients with the illustrations in Balupari and Rouch [21].

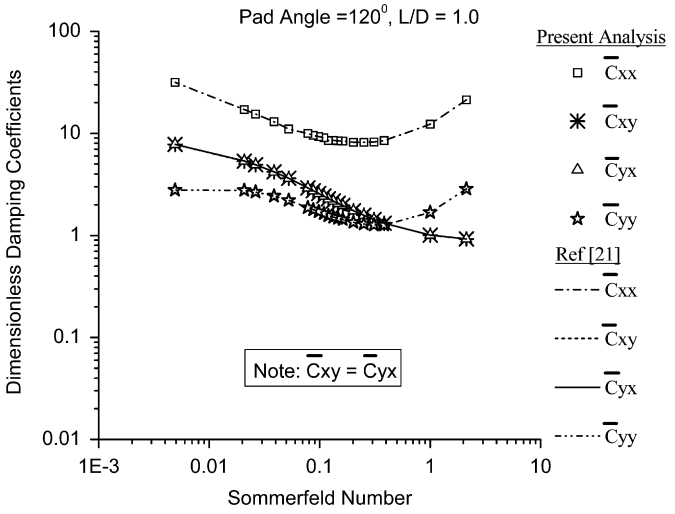

Fig. 3. Comparison of dimensionless damping coefficients with the illustrations in Balupari and Rouch [21].

7. Validation

An externally adjustable fluid film bearing will perform as a conventional partial arc bearing when both R_{adj} and T_{adj} are set to zero. Performance curves in Figs. 2 and 3 compare the results of present analysis with the illustrations in Balupari and Rouch [21], for a centrally loaded 120° conventional partial arc bearing with $L/D=1.0$ and operating with Re=1.

8. Results and discussions

Turbulence and clearance play an important role in deciding the bearing stability. For a known value of R_{adj} and T_{adj}, it is possible to have nine different positional configurations to the bearing element. However, the present analysis considers only the extreme positions, i.e., negative adjustment (i.e., $-R_{adj}$ and $-T_{adj}$) and positive adjustment (i.e., $+R_{adj}$ and $+T_{adj}$). Moreover, the

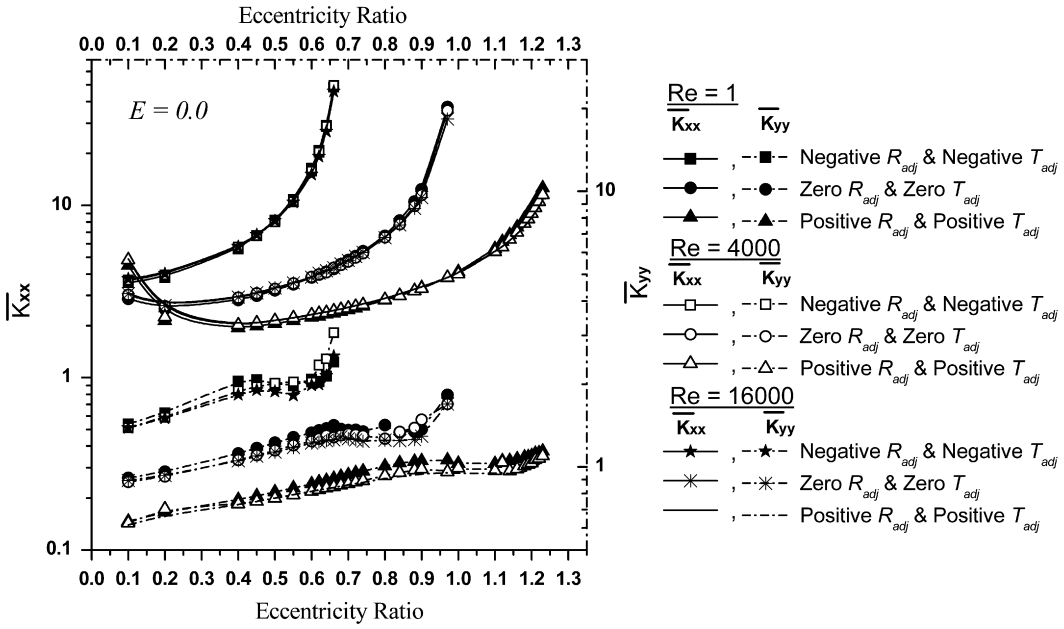

Fig. 4. Dimensionless K_{xx} and K_{yy} versus eccentricity ratio for various values of T_{adj} and R_{adj} for $E=0.0$.

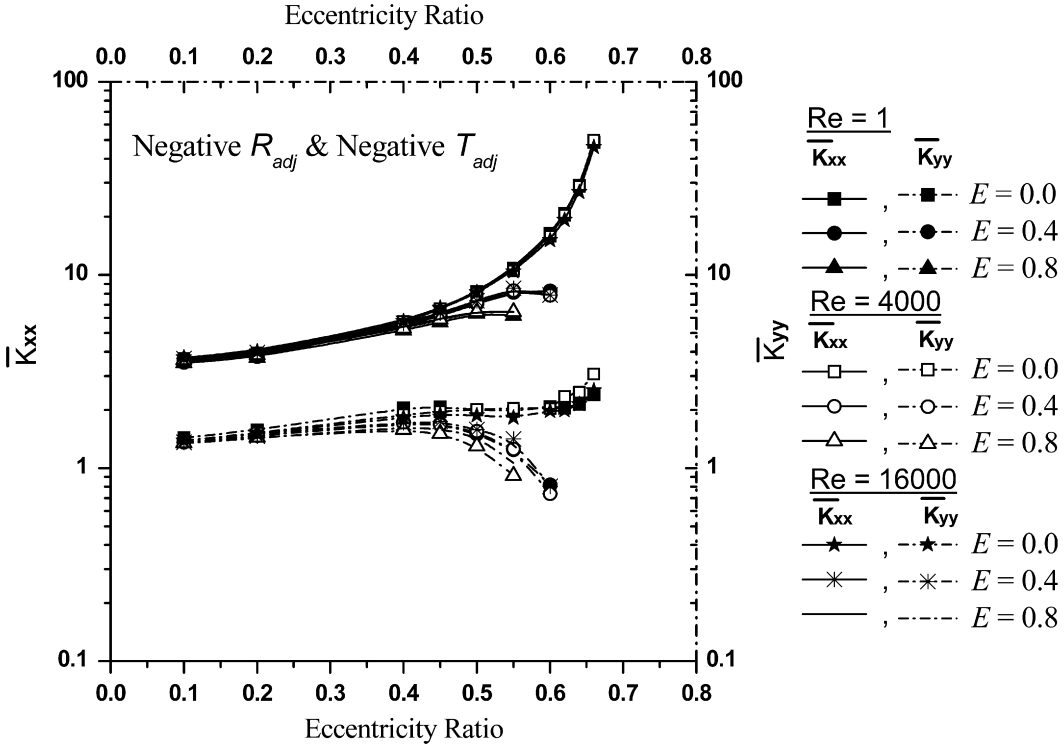

Fig. 5. Dimensionless K_{xx} and K_{yy} versus eccentricity ratio for various values of Re and E.

Sommerfeld number is dependent on adjustments [16]; eccentricity ratio is taken along the abscissa. Figs. 4–14 show the result of the present analysis for a bearing having R_{adj} of ± 0.25 C and δ of ± 0.0001065 rad.

Fig. 4 depicts that, for a given value of Reynolds number (Re) and eccentricity ratio, dimensionless direct stiffness coefficients are higher for a bearing with $-R_{adj}$ and $-T_{adj}$ than a conventional bearing. Moreover, for this adjustment configuration, an increase in ε significantly increases $\overline{K}_{xx}$, when compared with $\overline{K}_{yy}$. An increase in Re marginally reduces $\overline{K}_{xx}$, whereas a substantial reduction is observed in $\overline{K}_{yy}$. For $\varepsilon > 0.6$, $\overline{K}_{yy}$ is higher for a bearing with negative adjustments and operating in turbulent regime. From Fig. 5, it is observed that for a bearing with $-R_{adj}$ and $-T_{adj}$, at higher values of ε, Re in conjugation with E has a negative influence on dimensionless direct stiffness coefficients.

Fig. 6 shows that $\overline{K}_{xy}$ increases with $-R_{adj}$ and $-T_{adj}$. At lower ε, it is observed that $+R_{adj}$ and $+T_{adj}$ results in higher value of $\overline{K}_{xy}$ when compared with the one obtained with other adjustments. Moreover, an increase in ε gradually reduces $\overline{K}_{xy}$. On the other hand, at very high values of ε, a rise is observed in $\overline{K}_{xy}$. Furthermore, it is seen that, $\overline{K}_{xy}$ reduces marginally with an increase in Re and at lower values of ε, Re has negligible influence on $\overline{K}_{xy}$. Fig. 7 depicts that the adjustment configuration has major influence on $\overline{K}_{yx}$ than Re and E. At lower eccentricity ratio, it is seen that, $\overline{K}_{yx}$ is less for $+R_{adj}$ and $+T_{adj}$. Moreover, it is observed that, at higher ε, in laminar as well as in turbulent flow condition, $\overline{K}_{yx}$ is higher for $-R_{adj}$ and $-T_{adj}$. Fig. 8 shows that, for $-R_{adj}$ and $-T_{adj}$, an increase in E reduces the $\overline{K}_{xy}$ and it has marginal influence on $\overline{K}_{yx}$.

Fig. 9 demonstrates that dimensionless direct damping coefficients ($\overline{C}_{xx}$ and $\overline{C}_{yy}$) are higher with $-R_{adj}$ and $-T_{adj}$.

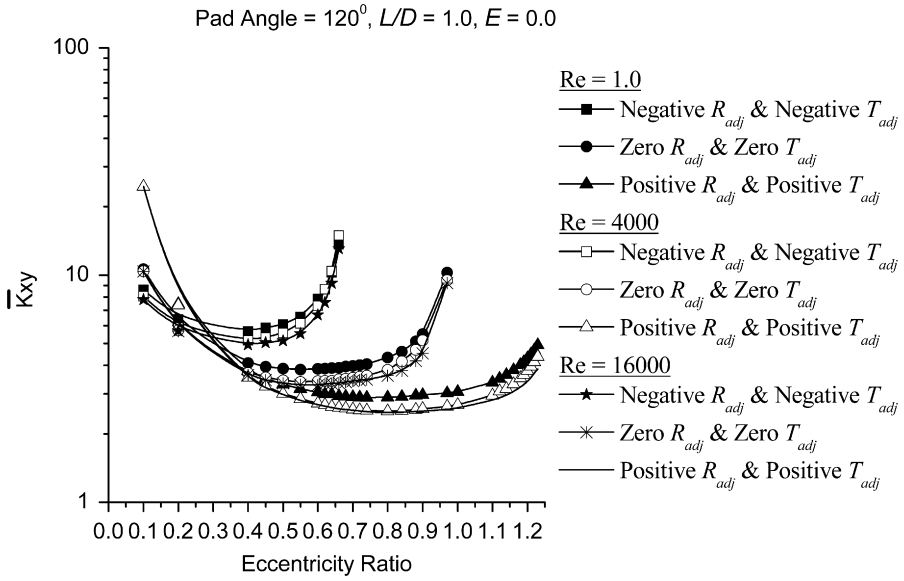

Fig. 6. Dimensionless K_{xy} versus eccentricity ratio for various values of T_{adj} and R_{adj} for $E=0.0$.

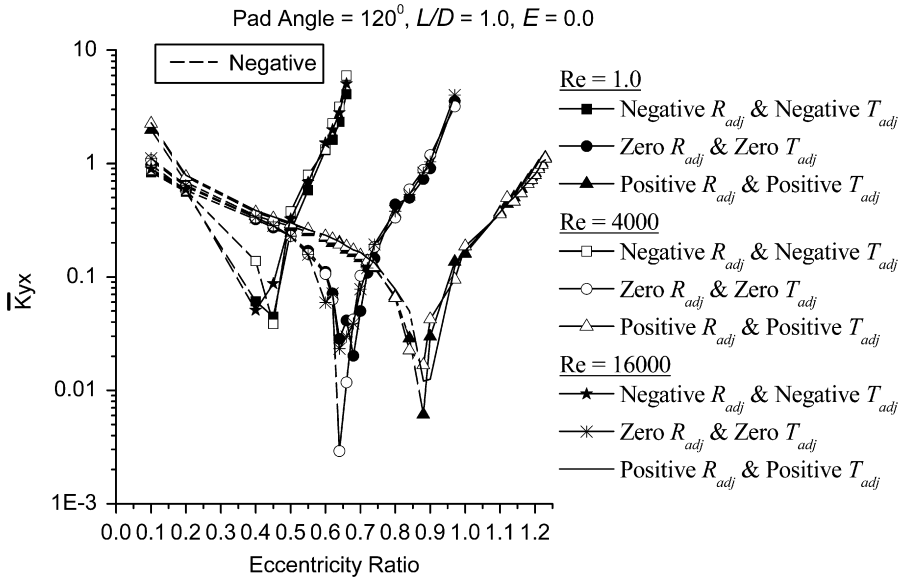

Fig. 7. Dimensionless K_{yx} versus eccentricity ratio for various values of T_{adj} and R_{adj} for $E=0.0$.

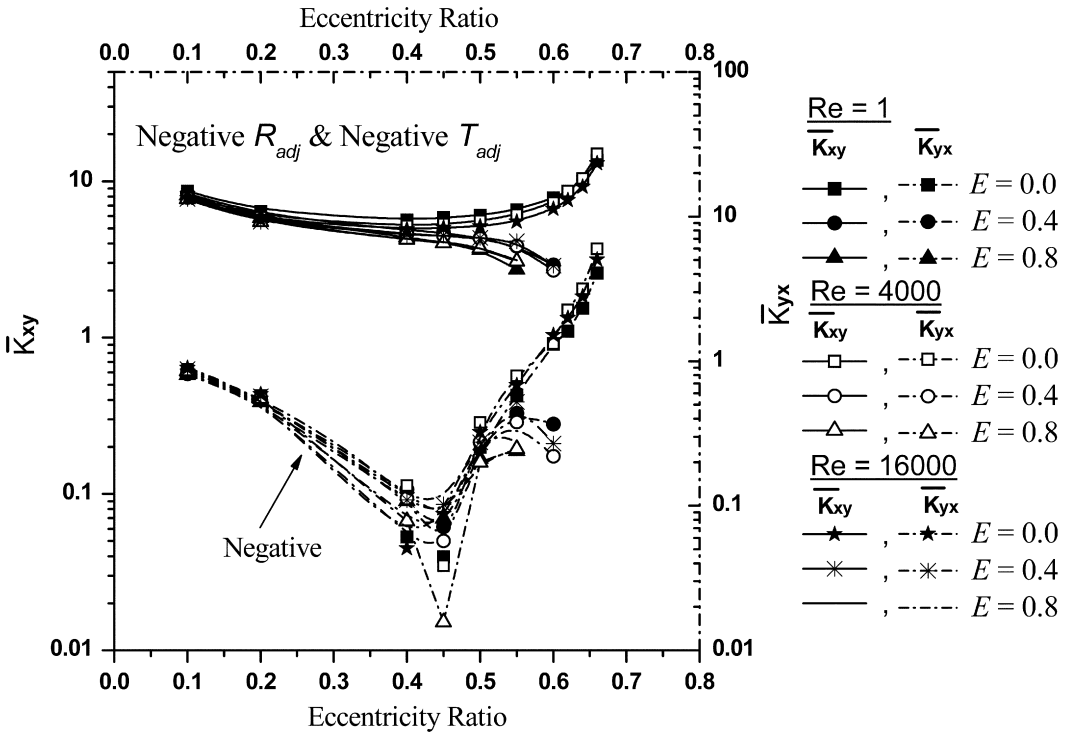

Fig. 8. Dimensionless K_{xy} and K_{yx} versus eccentricity ratio for various values of Re and E.

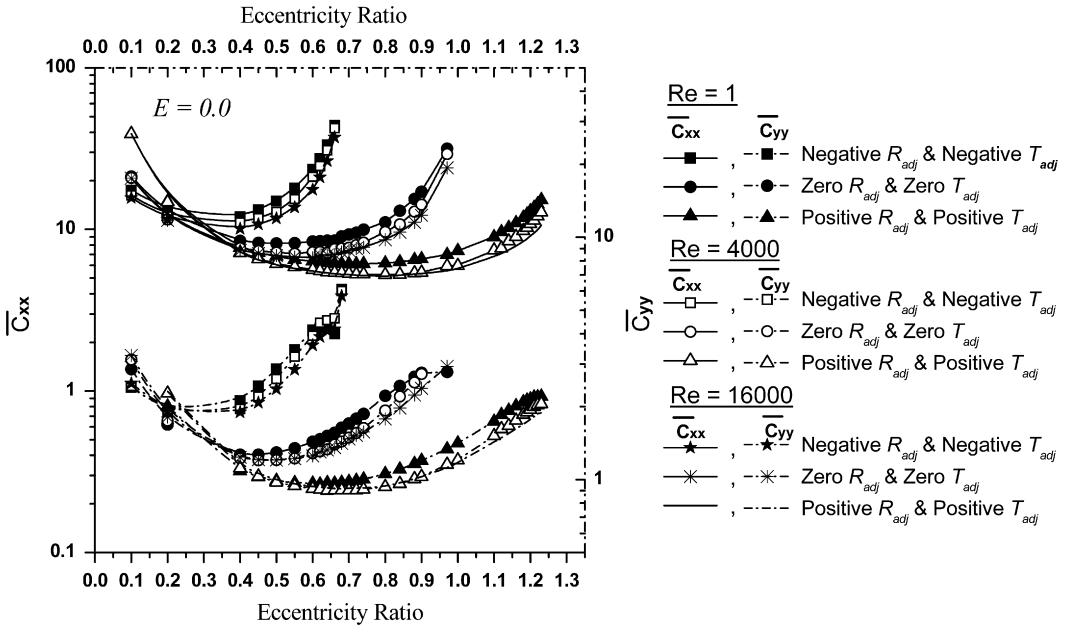

Fig. 9. Dimensionless C_{xx} and C_{yy} versus eccentricity ratio for various values of T_{adj} and R_{adj} for E=0.0.

However, at lower ε, it is observed that, $+R_{adj}$ and $+T_{adj}$, have higher $\overline{C}_{xx}$ and $\overline{C}_{yy}$. An increase in ε reduces dimensionless direct damping coefficients and at very high values of ε a rise is observed in dimensionless direct damping coefficients. Similarly, at lower values of ε, an increase in Re has minor influence on dimensionless direct damping coefficients. Fig. 10 reveals that dimensionless direct damping coefficients reduce substantially with an increase in Re and E, however, this reduction is prominent at higher values of ε.

From Figs. 11 and 12 it is seen that $\overline{C}_{xy}$ and $\overline{C}_{yx}$ are higher with negative $-R_{adj}$ and $-T_{adj}$ and increase with an increase in ε. A considerable reduction in $\overline{C}_{xy}$ and $\overline{C}_{yx}$ are observed with an increase in Re. At lower values of ε, an increase in Re from 1.0 to 4000 has greater influence on dimensionless cross-coupled damping coefficients than an increase in Re from 4000 to 16,000. At higher values of ε a rise in E reduces $\overline{C}_{xy}$.

Figs. 13 and 14 depicts that, in laminar as well as in turbulent flow condition, $-R_{adj}$ and $-T_{adj}$ have higher critical mass

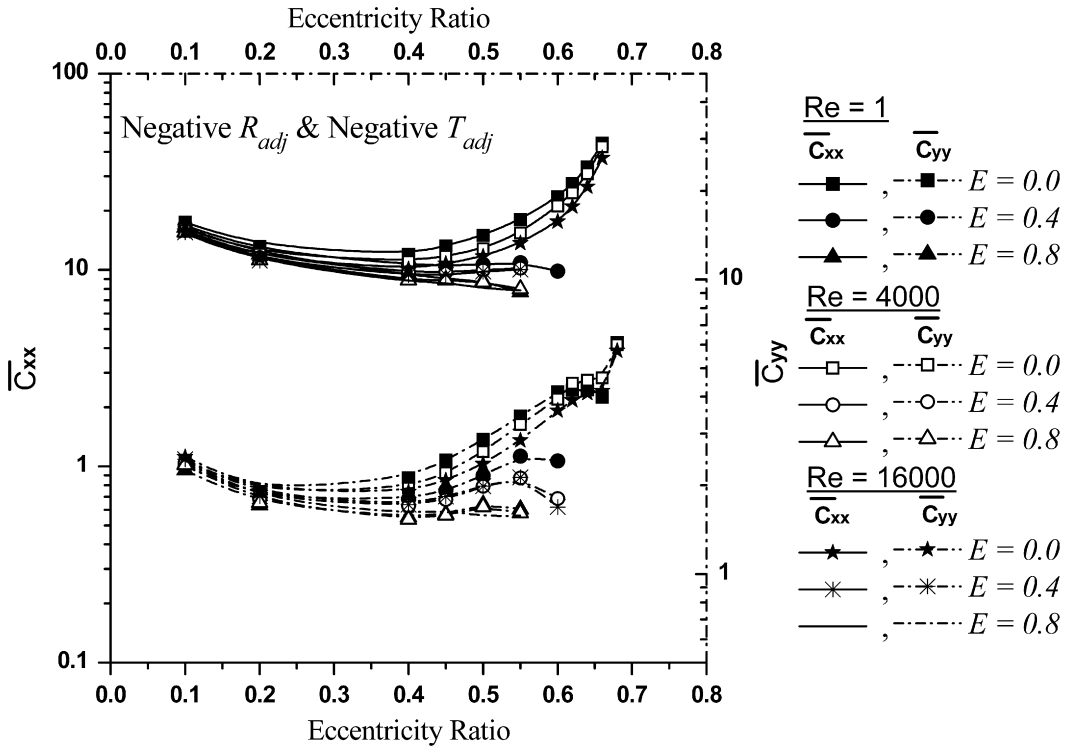

Fig. 10. Dimensionless C_{xx} and C_{yy} versus eccentricity ratio for various values of Re and E.

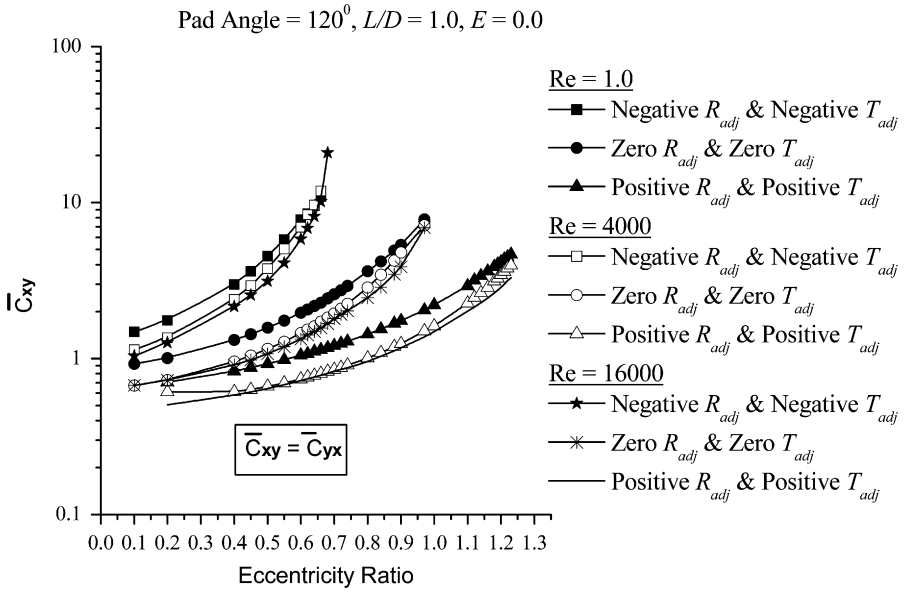

Fig. 11. Dimensionless C_{xy} versus eccentricity ratio for various values of T_{adj} and R_{adj} for E=0.0.

parameter than other adjustment configurations. From Fig. 13 it is seen that at lower eccentricity ratio, $+R_{adj}$ and $+T_{adj}$, configuration with Re=16,000 has higher critical mass parameter than a conventional bearing that is operating in the laminar flow regime. Moreover, it also seen that, the bearing with negative adjustment (i.e., $-R_{adj}$ and $-T_{adj}$) configuration and operating with Re=16,000 has the highest critical mass parameter than a bearing with other adjustment combinations. Similarly, a bearing with $+R_{adj}$ and $+T_{adj}$ configuration and operating in the laminar regime, offers least resistance to instability. Fig. 13 also demonstrates that at lower values of ε, the rotor-bearing system is susceptible to half frequency whirl. As ε increases a bearing with $-R_{adj}$ and $-T_{adj}$ offers higher stability to the rotor-bearing system than a conventional bearing. Moreover, $+R_{adj}$ and $+T_{adj}$ configuration has highest risk for instability. From Fig. 14 it is seen that an increase in E reduces the mass parameter, which in turn reduces the stability of the rotor-bearing system.

9. Conclusion

The influence of turbulence on dynamic performance characteristics of an externally adjustable bearing is presented in this paper. The bearing clearance and the turbulence have significant influence on the stability of the rotor dynamic system. By varying the film thickness and its gradient in the circumferential direction, it is possible to control the bearing stability. In an externally adjustable bearing, a negative radial adjustment (R_{adj}) reduces the bearing radial clearance and further a negative tilt adjustment (T_{adj}) narrows down the convergent zone of the fluid film in circumferential direction. This adjustment configuration of the bearing element results in superior stability characteristics, thereby improving the dynamic coefficients of the bearing. On the other hand, $+R_{adj}$ and $+T_{adj}$ increase the value of minimum film thickness. High values of minimum film thicknesses when accompanied by low values of the eccentricity ratio produce a large diverging film shapes at the leading edge of the bearing for

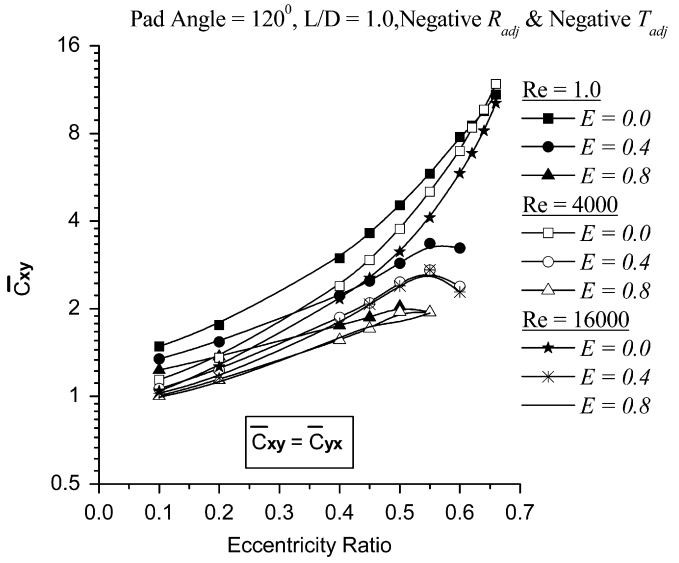

Fig. 12. Dimensionless C_{xy} versus eccentricity ratio for various values of Re and E.

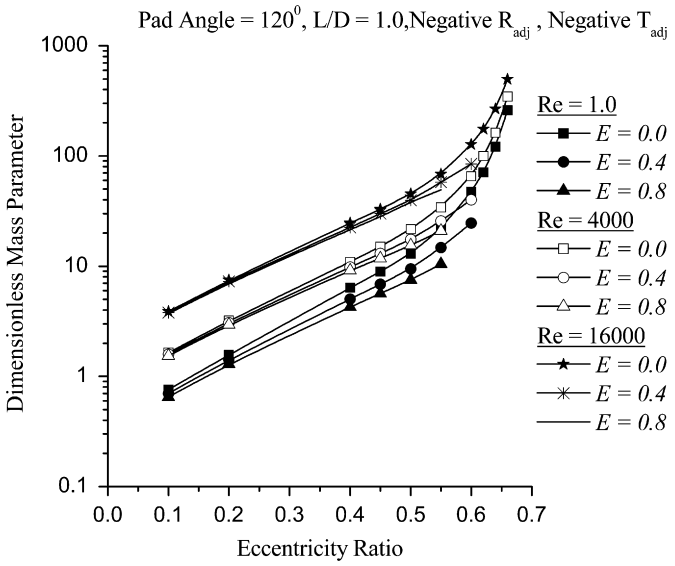

Fig. 14. Critical mass parameter versus eccentricity ratio for various values of Re and E.

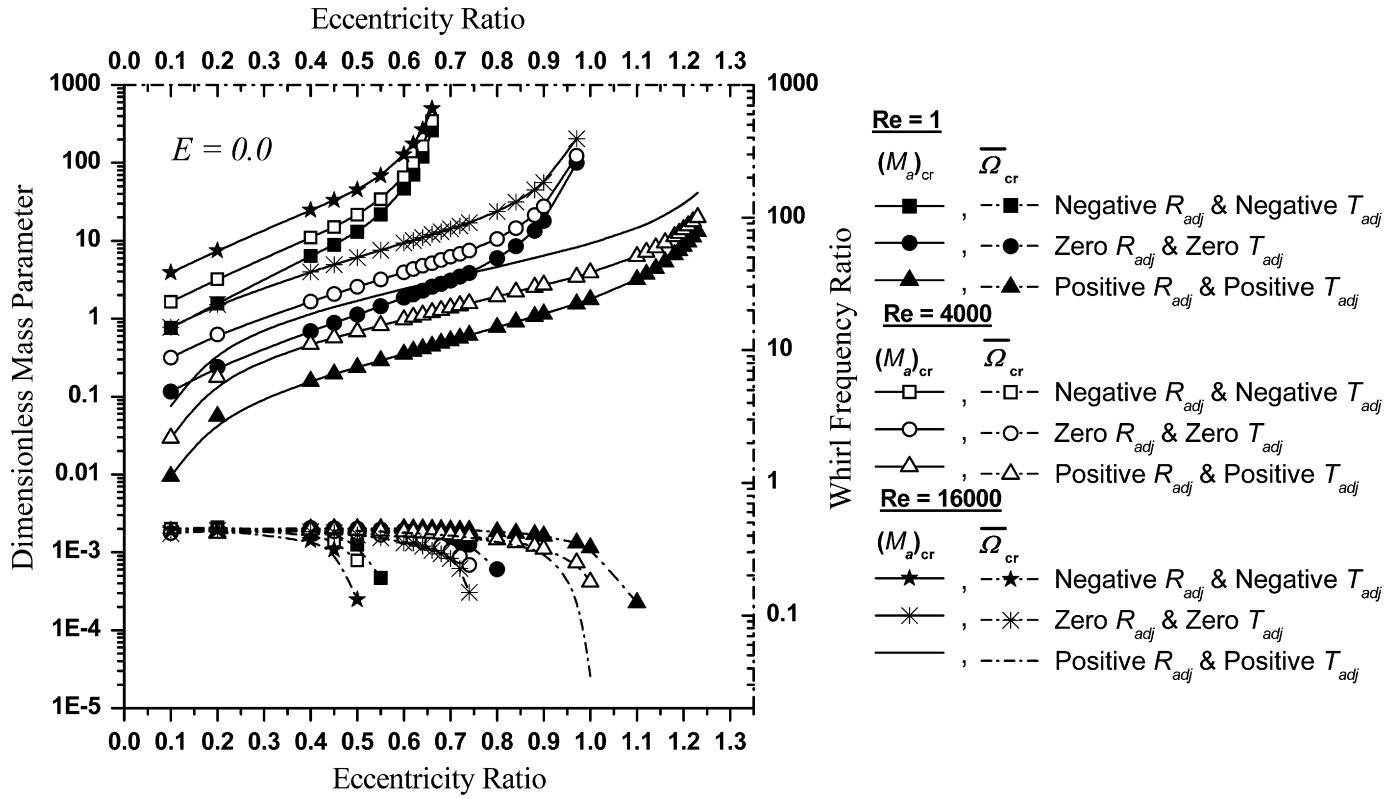

Fig. 13. Critical mass parameter and whirl frequency ratio versus eccentricity ratio for various values of T_{adj} and R_{adj} for E=0.0.

which condition the operation may be unstable. At higher values of eccentricity ratio, the bearing with negative radial and negative tilt adjustment configuration and operating in turbulent regime has greater stability than a conventional bearing operating under similar conditions.

References

[1] Pai R, Parkins DW. Measurement of eccentricity and attitude angle of a journal bearing. In: Proceedings of the third national conference on fluid machinery, Pune, September 12–13; 1998. p. 181–8.

[2] Akkok M, Ettles CM. The effect of grooving and bore shape on the stability of journal bearings. ASLE Trans 1980;23(4):431–41.

[3] Schuller, FT. Effect of number of lobes and length–diameter ratio on the stability of tilted-lobe hydrodynamic journal bearings at zero load. Technical Report, NASA TN D—7902, 1975. p. 5.

[4] Schuller FT. Stability experiments with Hydrodynamic-tilted lobe journal bearings of various number of lobes and length-to-diameter ratios. ASLE Trans 1977;20:271–81.

[5] Malik M, Chandra M, Sinhasan R. Performance characteristics of titled three-lobe journal bearing configurations. Tribol Int 1981;14(6):345–50.

[6] Malik M, Chandra M, Sinhasan R. Design data for three-lobe bearings. ASLE Trans 1981;24(3):345–53.

[7] Malik M. The analysis of symmetric and tilted four-lobed journal bearing configurations. ASLE Trans 1983;26(2):264–9.

[8] Akkok M, Ettles CM McC, Safar ZS. The effect of grooving and bore shape on the stability of journal bearings. ASLE Annual Conference, St. Loius, 79-AM-6D-2, 1979. p. 1–5.

[9] Soni Z, Sinhasan R, Singh DV. Performance characteristics of noncircular bearings in laminar and turbulent flow regimes. ASLE Trans 1981;24:29–41.

[10] Martin JK. A mathematical model and numerical solution technique for a novel adjustable hydrodynamic bearing. Int J Numer Methods Fluids 1999;30:845–64.

[11] Martin JK, Parkins DW. Testing of a large adjustable hydrodynamic journal bearing. STLE Tribol Trans 2001;44(4):559–66.

[12] Martin JK, Parkins DW. Theoretical studies of continuously adjustable hydrodynamic fluid film bearing. ASME J Tribol 2002;124:203–11.

[13] Martin JK. Extended expansion of the Reynolds equation. Proc Inst Mech Eng Part J: J Eng Tribol 2002;216(1):49–51.

[14] Martin JK. Measuring the performance of a novel fluid film bearing supporting a rotor on a stationary shaft, by non-contacting means. Proc Inst Mech Eng Part K: J Multi-body Dyn 2004;218(3):143–51.

[15] Shenoy BS, Pai R. Steady state performance characteristics of a single pad externally adjustable fluid film bearing. J Adv Mech Des Syst Manufact 2008;2(5):937–48.

[16] Shenoy BS, Pai R. Steady state performance characteristics of a single pad externally adjustable fluid film bearing in the laminar and turbulent regimes. ASME J Tribol 2008;131. doi:10.11115/1.3070580.

[17] Taylor CM, Dowson D. Turbulent lubrication theory-application to design. ASME J Lubr Technol 1974;96:36–47.

[18] Ng CW, Pan CHT. A linearized turbulent lubrication theory. ASME J Basic Eng 1965;87:675–88.

[19] Pinkus O, Bupara SS. Adiabatic solutions for finite journal bearings. ASME J Lubr Technol 1979;101:492–6.

[20] Hamrock BJ. Fundamentals of fluid film lubrication. Mechanical engineering series. McGRAW-HILL International Editions; 1994.

[21] Balupari RS, Rouch K. Validation of finite element program for journal bearings—static and dynamic properties. Master's Thesis, Graduate School of the University of Kentucky, 2004.